FULL PAPER

The Role of Fullerene Mixing Behavior in the Performance of Organic Photovoltaics: PCBM in Low-Bandgap Polymers

*Huipeng Chen, Jeff Peet, Sheng Hu, Jason Azoulay, Guillermo Bazan, and Mark Dadmun**

This manuscript reports the mixing behavior, interdiffusion, and depth profile of 1-[3-(methoxycarbonyl)propyl]-1-phenyl-[6,6]C_{61} (PCBM):low-bandgap (LBG) polymer thin films that are formed by thermally annealing initial bilayers. The extent of mixing of PCBM is higher in polymers that include the 2,1,3-benzothiadiazole (BT) unit than in polymers that incorporate the 2,1,3-benzooxadiazole (BO) unit. This difference is ascribed to the enhanced mixing behavior of PCBM with the benzothiadiazole functionality than with benzooxadiazole functionality, which is attributed to preferred intermolecular interactions. The increased polymer/fullerene mixing is found to be crucial for optimal device performance. A decrease of polymer/fullerene mixing reduces the donor/acceptor interface, which lowers the probability of exciton dissociation and charge generation. Moreover, low PCBM mixing provides limited pathways for electron transport out of a miscible region, due to long distances between adjacent PCBM in such a miscible phase. This inhibits electron transport and increases the recombination of free charge carriers, resulting in a decrease in short circuit current and device performance. These results further exemplify the importance of the thermodynamic mixing behavior of the polymer:fullerene pair in designing next-generation conjugated polymers for organic photovoltaic (OPV) applications, as this controls the final morphology of the OPV active layer.

1. Introduction

One of the most important challenges facing our society is the development of renewable and environmentally clean energy which could supplant our reliance on fossil fuels. Polymer based bulk-heterojunction (BHJ) photovoltaic cells, based on blends of conjugated polymers (CP) and fullerenes, are one potential economically viable option for low cost renewable power generation. It is believed that commercializing organic solar cells requires power conversion efficiencies above 10% and long lifetimes while present power conversion efficiencies approach this value in a laboratory setting.[1] Efficiencies greater than 10% are expected when the losses associated with exciton dissociation and collection are minimized,[2] which is strongly associated with improvements in the morphological characteristics of polymer:fullerene BHJs. While there is a tremendous body of literature on the development of new low-bandgap (LBG) semiconducting polymers that have higher potential efficiency, there is relatively little that has been done to probe the fundamental nature of the polymer/fullerene mixture or how the structure of the polymer might affect this.[3]

Neutron scattering has been instrumental in developing a recent paradigm shift in the understanding of the structure of conjugated polymer/fullerene mixtures, as the neutron scattering length density (SLD) of a protonated matrix differs significantly from that of the fullerene. The SLD of the fullerene is similar to that of deuterated organic compounds. Recent work by our group[4,5] and others[6–9] has shown that these mixtures are much more miscible than originally thought. For instance, our neutron reflectivity and small angle neutron scattering studies of the model OPV system poly(3-hexylthiophene) (P3HT) mixed with the surface-functionalized fullerene 1-(3-methyloxycarbonyl)propy(1-phenyl [6,6] C61 (PCBM) demonstrate miscibility up to 22% PCBM.[5] Moreover, this level of miscibility requires a new model of the molecular level organization of the fullerene and conjugated polymer and a method to correlate this model to charge transport in OPV active layers.[4] The ideal morphology for an OPV active layer is often described as a bicontinuous, interpenetrating network that consists of

Dr. H. P. Chen, Prof. M. Dadmun
Department of Chemistry
University of Tennessee
Knoxville, TN, 37996, USA
Prof. M. Dadmun
Chemical Sciences Division
Oak Ridge National Lab
Oak Ridge, TN, 37831, USA
Dr. J. Peet
Konarka Technologies
Lowell, MA, 01852, USA
S. Hu
Department of Chemical and Biomolecular Engineering
University of Tennessee
Knoxville,TN, 37996, USA
Dr. J. Azoulay, Prof. G. Bazan
Center for Polymers and Organic Solids
The University of California
Santa Barbara, CA, 93016, USA

DOI: 10.1002/adfm.201300862

pure donor and acceptor phases. In this picture, excitons dissociate at the donor/acceptor interfaces to generate free charge carriers that flow into the pure donor or acceptor phase and then to the electrodes. However, this miscibility means that these two pure phases cannot co-exist and the role of this miscible phase in the operation of the active layer is not clear. For instance, significant free charge carriers will be generated in the miscible region due to the abundant donor/acceptor interfacial area in this miscible phase, but transport of these free charges to the electrodes is not as efficient as in the pure phases. Thus, if there is sufficient acceptor loading in the miscible phase, the proposed model envisions these free charge carriers can flow as 'streams' into pure donor or acceptor phases where they efficiently transport to the electrodes. Therefore, the benefit of the miscible phase is that it provides a plethora of donor-acceptor interface for efficient exciton dissociation, but also requires sufficient mixing to allow charge transport. This model is derived based on the behavior of the archetypal P3HT:PCBM bulk heterojunction. However, the most promising new conjugated polymer:fullerene active layers in organic photovoltaics utilize low band-gap donor-acceptor copolymers, such as the heavily studied poly(4,4-dioctyldithieno(3,2-b:2′,3′-d)silole)-2,6-diyl-alt-(2,1,3-benzothiadiazole)-4,7-diyl) (PSBTBT) and poly[*N*-9″-hepta-decanyl-2,7-carbazole-alt-5,5-(4′,7′-di-2-thienyl-2′,1′,3′-benzothiadiazole)] (PCDTBT) polymers.[10–15] Unfortunately, there has been very little correlation of photovoltaic activity to the morphology, structure, and especially miscibility of these promising bulk heterojunctions and structurally similar materials.[13,14,16]

Therefore, there is a clear need to understand the relationship between chemical structure of conjugated polymer and its mixing behavior with fullerenes to rationally optimize the design of conjugated polymers for use in organic photovoltaics. For instance, many of the newer low bandgap conjugated polymers are "donor-acceptor" copolymers that incorporate a benzothiadiazole (BT) acceptor unit or the similar benzooxadiazole (BO) unit. The BO unit is utilized as its presence increases the open-circuit voltage (V_{oc}) without significantly altering the absorption onset, which, if all other characteristics are equivalent, should result in increased solar cell performance. However, the performance of these materials is no better and often worse than the corresponding polymers with the BT unit, which is usually ascribed to "poor morphology".[17–19] Unfortunately, the definition of 'poor morphology', what causes this poor morphology, and the correlation of this poor morphology to charge transport and OPV performance are lacking. Therefore, a more complete and accurate measurement of the mixing behavior and interfacial structure of a set of polymer:fullerene blends to elucidate the role of the presence of the BO and BT units on the mixing behavior of these blends will provide crucial fundamental information that can be used to guide future conjugated polymer design for OPV active layers.

In the present work, we report an investigation of the extent of mixing of PCBM in a series of donor–acceptor copolymers that incorporate benzothiadiazole (BT) or benzooxadiazole (BO) units. The conjugated polymer pairs are chosen so that two polymers are identical except for the substitution of the BO unit for the BT unit in the polymer backbone. The mixing behavior is determined by the change in the depth profile of PCBM in CP:PCBM bilayers with thermal annealing, which are monitored by neutron reflectivity. As shown in our previous work, this protocol quantifies the ability of the PCBM to mix into the conjugated polymer layer, where the amount of PCBM in the conjugated polymer layer after heating is interpreted as the extent of the fullerene mixing in the conjugated polymer.[5] This is because only the PCBM that is thermodynamically driven to mix into the CP layer will diffuse into the polymer when thermally annealed.

Therefore, in the present work, we report the results of experiments that determine the mixing behavior of PCBM with low bandgap polymers to provide previously unavailable information correlating the extent of mixing of these two components to charge transport and OPV performance as well as delivering fundamental insight into the role of CP structure on its mixing behavior with fullerenes.

2. Results and Discussion

2.1. Mass Density and Scattering Length Density of Conjugated Polymers

Table 1 lists the mass density of all the LBG polymers obtained from pycnometry, which indicates that replacing the BT unit of the copolymer with the BO unit does not significantly alter the density of the materials. The experimentally determined SLD of the LBG polymers as determined from neutron reflectivity and the calculated SLD based on the density and atomic composition of LBG polymers are listed in Table 1 as well, which are in agreement with each other. The SLD of the polymers containing the BO unit are slightly higher than the corresponding polymer that contains the BT unit, which is because of the higher SLD of oxygen than that of sulfur.

2.2. Mixing Behavior of PCBM in PSBTBT and SOEH

PSBTBT and SOEH are LBG polymers that have the exact same chemical structure except that the BT unit in PSBTBT is replaced with a BO unit in SOEH. (**Table 2**) The experimentally determined specular neutron reflectivity of the as-cast and thermally annealed samples along with that of the fitted model of the PSBTBT:PCBM bilayer are presented in **Figure 1**. As shown in Figure 1, the reflectivity of the as-cast PSBTBT:PCBM bilayer exhibits the Kiessig fringes that indicate the bilayer structure of this film. The damping of these Kiessig fringes are observed after the sample is annealed

Table 1. Experimental scattering length density (SLD^e), calculated scattering length density (SLD^c) and density of the conjugated polymers.

	PSBTBT (BT)	SOEH (BO)	PCPDTBT (BT)	COEH (BO)	PCDTBT (BT)	PCDTBX (BO)
SLD^e [$\times 10^6$ A^{-2}]	1.12	1.21	1.12	1.15	1.51	1.62
SLD^c [$\times 10^6$ A^{-2}]	1.13	1.20	1.13	1.17	1.53	1.60
Density [g/cm^3]	1.17	1.16	1.10	1.07	1.22	1.22

Table 2. Chemical structure, name, and abbreviation of the LBG polymers, 2,1,3-Benzothiadiazole (BT_m), and 2,1,3-Benzooxadiazole (BO_m).

Chemcial structure	Name	Abbreviation	M_n (kDa); PDI
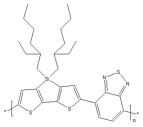	Poly(4,4-dioctyldithieno(3,2-b:2′,3′-d) silole)-2,6-diyl-alt-(2,1,3-benzothiadiazole)-4,7-diyl)	PSBTBT	27; 2,4
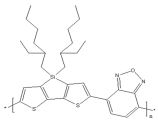	Poly(4,4-dioctyldithieno(3,2-b:2′,3′-d) silole)-2,6-diyl-alt-(2,1,3-benzooxadiazole)-4,7-diyl)	SOEH	25; 2.7
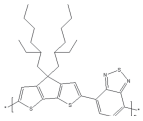	Poly[2,6-(4,4-bis-(2-ethylhexyl)-4H-cyclopenta [2,1-b;3,4-b′]dithiophene)-alt-4,7(2,1,3-benzothiadiazole)]	PCPDTBT	70; 2.5
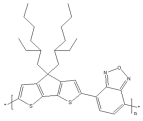	Poly[2,6-(4,4-bis-(2-ethylhexyl)-4H-cyclopenta [2,1-b;3,4-b′]dithiophene)-alt-4,7(2,1,3- benzooxadiazole)]	COEH	30; 2.0
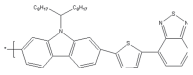	Poly[N-9″-hepta-decanyl-2,7-carbazole-alt-5,5-(4′,7′-di-2-thienyl-2′,1′,3′-benzothiadiazole)]	PCDTBT	39; 2.7
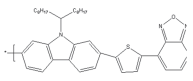	Poly[N-9″-hepta-decanyl-2,7-carbazole-alt-5,5-(4′,7′-di-2-thienyl-2′,1′,3′-benzooxadiazole)]	PCDTBX	34; 2.1
	2,1,3-Benzothiadiazole	BT_m	
	2,1,3-Benzooxiadiazole	BO_m	

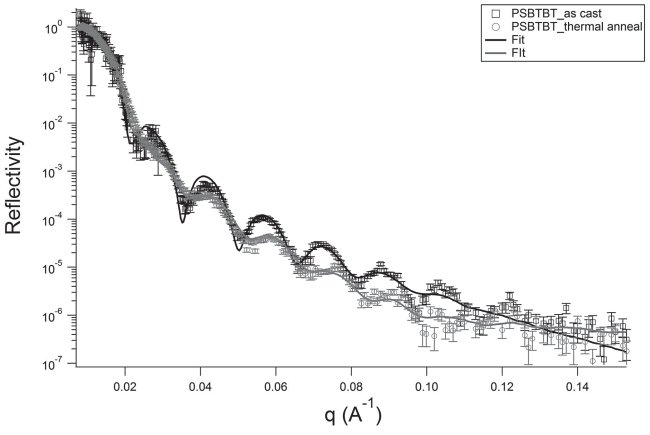

Figure 1. Reflectivity curves of the PSBTBT:PCBM bilayer as cast and thermally annealed. The lines are fits to model scattering length density profiles.

at 140 °C for 30 min, which indicates the roughening of the PSBTBT-PCBM interface and interdiffusion of PCBM into PSBTBT. The resultant PCBM depth profiles for the as-cast and thermally annealed samples are shown in **Figure 2**, which further verifies this interpretation and shows how the depth profiles change from the initially well-separated PSBTBT and PCBM individual layers to mixed layers as the PCBM infuses into the PSBTBT layer with thermal annealing. With thermal annealing, PCBM readily diffuses into the PSBTBT, forming a plateau region at $z \approx 220$–360 Å which consists of 23 vol% PCBM, which indicates the presence of a homogeneous mixture of PSBTBT and PCBM.

Moreover, this portion of the thin film is not impacted by the air or silicon surface, and therefore describes the extent of PCBM mixing in PSBTBT. Thermal annealing allows the initially fully separated PCBM and PSBTBT to interdiffuse *only* if there exists a thermodynamic driving force for the two components to do so. Furthermore, this extent of mixing is similar to

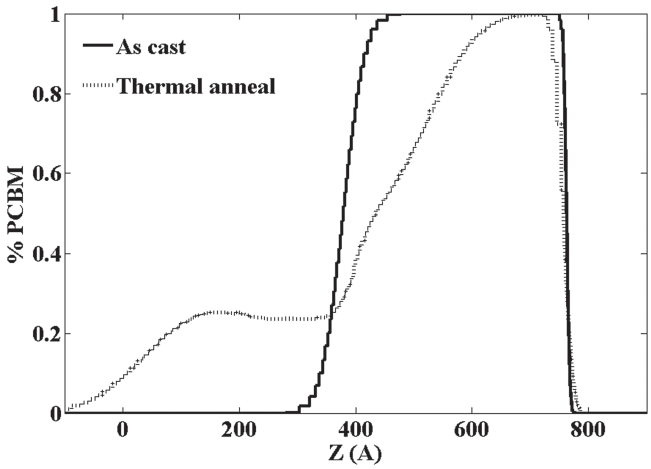

Figure 2. PCBM depth profile of the PSBTBT:PCBM bilayer as-cast and thermally annealed as determined from the reflectivity curves shown in Figure 1.

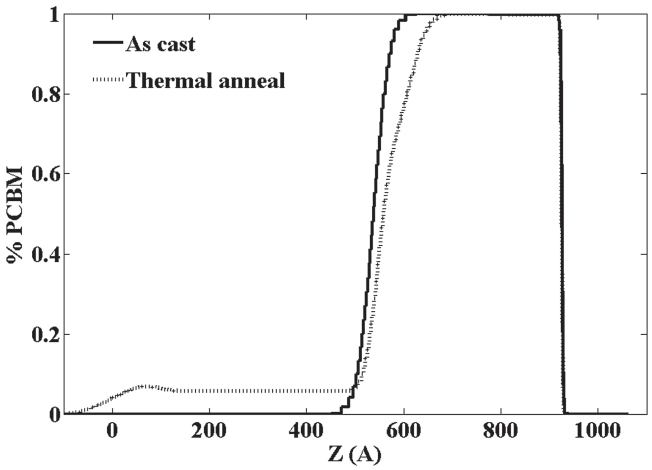

Figure 4. PCBM volume fraction profile of the SOEH:PCBM bilayer as cast and thermally annealed as determined from the reflectivity curves shown in Figure 3.

previously reported values.[13,16] Russell and coauthors reported a extent of mixing of 19 vol% and Ade and coauthors reported a value of 26(±2) vol%.[13,16] Inspection of this depth profile also shows that the PCBM selectively segregates to just below the air surfaces in this thin film, which is consistent with previously reported results in P3HT:PCBM mixtures from our group[5] and others.[20–22]

The reflectivity of the SOEH:PCBM bilayer is presented in **Figure 3**, also exhibiting the Kiessig fringes that indicate the bilayer nature of the structure before annealing. The damping of the oscillations is also observed for SOEH:PCBM bilayers with thermal annealing at 140 °C for 30 min, but the damping is much weaker than that of the thermally annealed PSBTBT:PCBM bilayers, which may indicate less interdiffusion of PCBM into SOEH. The PCBM depth profiles of SOEH:PCBM bilayer are presented in **Figure 4**. These results show that with thermal annealing, PCBM readily diffuses into SOEH, forming a plateau region at $z \approx 130$–480 Å consisting of 6 vol% PCBM. This represents the extent of PCBM mixing with SOEH and is much less than the extent of PCBM mixing with PSBTBT, our first indication that the inclusion of the BO unit inhibits the mixing of PCBM with the conjugated polymer.

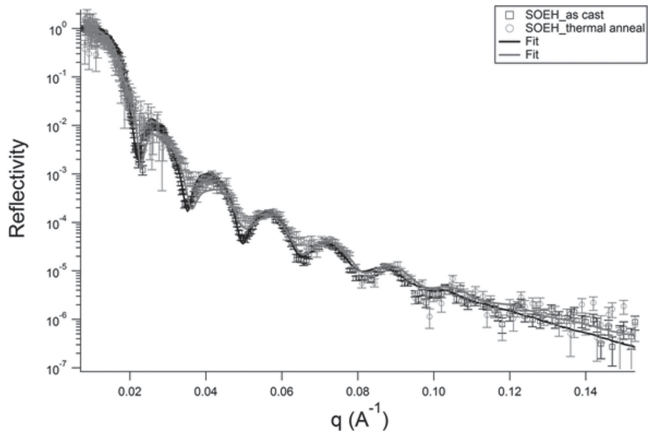

Figure 3. Reflectivity curves SOEH:PCBM bilayer of as cast and thermally annealed samples. The lines are fits to model scattering length density profiles.

2.3. Mixing Behavior of PCBM in PCPDTBT and COEH

To further investigate the role of the chemical structure of the conjugated polymer on its mixing behavior with PCBM, the evolution of the depth profiles of PCPDTBT:PCBM and COEH:PCBM bilayers with thermal annealing are monitored. In this pair, the Si bridging atom of PSBTBT and SOEH are replaced with a carbon atom. Also, similar to the PSBTBT and SOEH pair, the structures of PCPDTBT and COEH are identical except that PCPDTBT contains a benzothiadiazole unit where COEH contains benzooxadiazole.

The reflectivity of the PCPDTBT:PCBM bilayer is presented in **Figure 5**, exhibiting the Kiessig fringes that indicate the bilayer nature of the structure before annealing. Similar to the PSBTBT bilayer, the damping of Kiessing fringes is also observed for the PCPDTBT:PCBM bilayer with thermal annealing at 140 °C for 30 min, which indicates the interdiffusion of PCPDTBT and PCBM. The PCBM depth profiles of PCPDTBT:PCBM bilayer before and after thermal annealing are presented in **Figure 6**. With thermal annealing, PCBM diffuses into PCPDTBT, forming a plateau region at $z \approx 180$–400 Å that consists of 9 vol% PCBM, which is the extent of PCBM mixing with PCPDTBT at 140 °C.

The reflectivity of the COEH:PCBM bilayer is presented in **Figure 7**, showing similar behavior as the previously presented samples, modest damping of initial Kiessing fringes with thermal annealing indicating the interdiffusion of PCBM and PCPDTBT. The PCBM depth profiles of the COEH:PCBM bilayers are presented in **Figure 8**. The initial bilayer is well separated with thicknesses of PCBM and COEH *ca*. 400 Å and

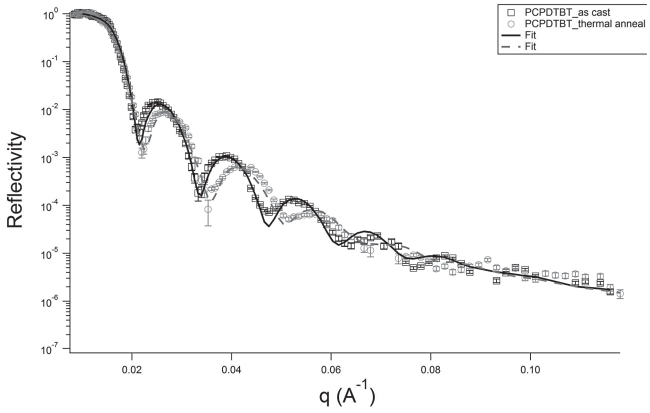

Figure 5. Reflectivity curves PCPDTBT:PCBM bilayer of as-cast and thermally annealed samples. The lines are fits to model scattering length density profiles.

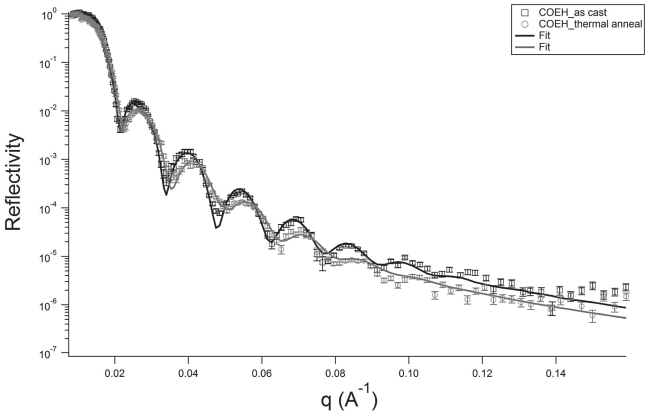

Figure 7. Reflectivity curves COEH:PCBM bilayer of as-cast and thermally annealed samples. The lines are fits to model scattering length density profiles.

600 Å, respectively. A very small amount PCBM diffuses into COEH after thermal annealing, resulting in a plateau region at $z \approx 130$–520 Å with a loading of only 3 vol% PCBM. Therefore, PCBM is much less miscible in COEH than in its BT counterpart, PCPDTBT. Moreover, the substitution of the Si atom in PSBTBT and SOEH for a carbon atom in PCPDTBT and COEH also results in a lowering of the extent of PCBM mixing with the polymer matrix.

2.4. Mixing Behavior of PCBM in PCDTBT and PCDTBX

PCDTBT and PCDTBX are the third pair of CPs with similar chemical structure that are examined, where the only difference is the replacement of the BT unit of PCDTBT with BO in PCDTBX. For these two LBG polymers, a nitrogen atom is the bridging atom on the main chain. The reflectivity of the PCDTBT:PCBM bilayer is presented in **Figure 9**, exhibiting the Kiessig fringes that indicate the bilayer nature of the structure before annealing. A significant damping of the Kiessing fringes is observed for the PCDTBT:PCBM bilayers with thermal annealing, which indicates a strong interdiffusion of PCBM into PCDTBT. The PCBM depth profiles of PCDTBT:PCBM bilayer are presented in **Figure 10**, which verifies that with thermal annealing, PCBM diffuses into PCDTBT. This depth profile exhibits a concentration plateau region at $z \approx 320$–600 Å with an extent of PCBM mixing in PCDTBT of 17 vol% at 140 °C.

The reflectivity and PCBM depth profiles of PCDTBX:PCBM bilayer are presented in **Figure 11** and **Figure 12**. A small change in the reflectivity curve is observed with thermal annealing, which translates to PCBM depth profiles with a plateau region at $z \approx 160$–460 Å and a loading of 3% PCBM after thermal annealing. This, as with the other samples, indicates that only 3 vol% PCBM can dissolve in PCDTBX at 140 °C.

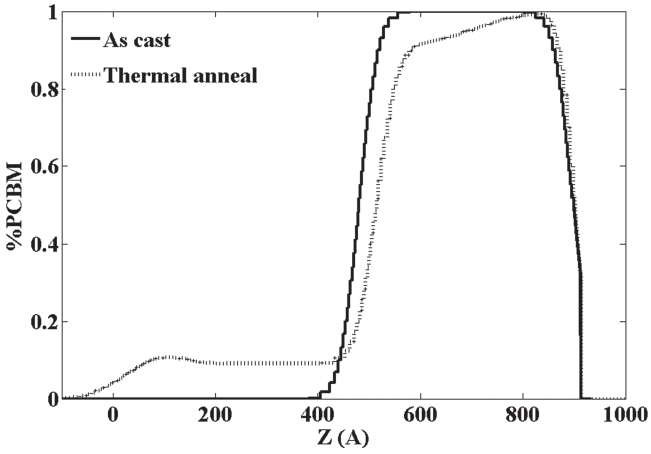

Figure 6. PCBM depth profile of the PCPDTBT:PCBM bilayer as-cast and thermally annealed as determined from the reflectivity curves shown in Figure 5.

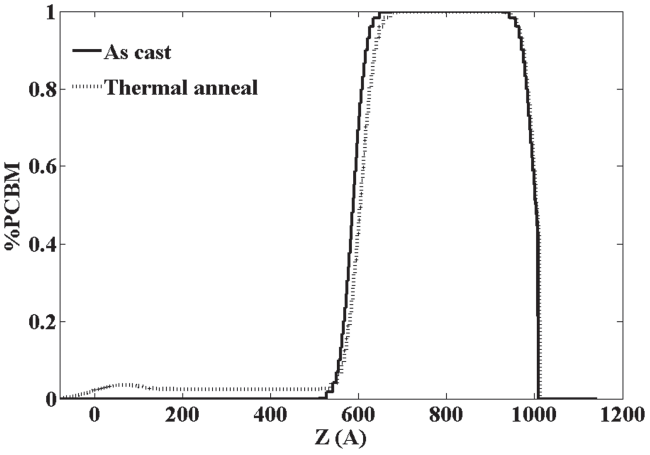

Figure 8. PCBM volume fraction profile of the COEH:PCBM bilayer as cast and thermally annealed as determined from the reflectivity curves shown in 7.

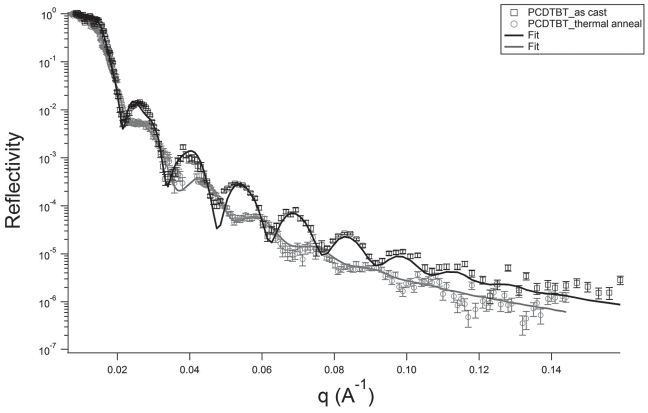

Figure 9. Reflectivity curves PCDTBT:PCBM bilayer of as-cast and thermally annealed samples. The lines are fits to model scattering length density profiles.

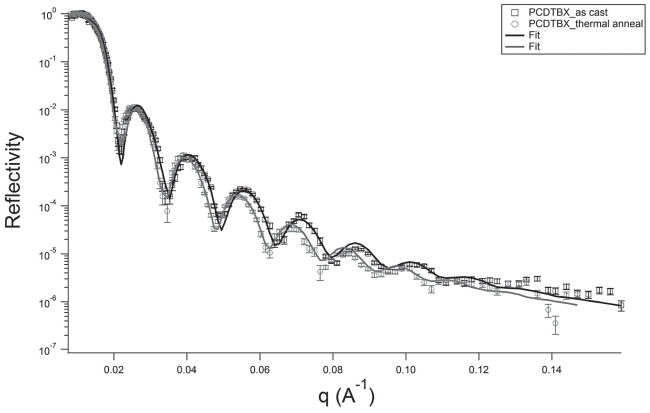

Figure 11. Reflectivity curves of the PCDTBX:PCBM bilayer as cast and thermally annealed samples. The lines are fits to model scattering length density profiles.

2.5. Solubility of PCBM in 2,1,3-Benzothiadiazole and 2,1,3-Benzooxadiazole

The mixing ability of PCBM in all the polymers are listed in **Table 3**, which shows that in all cases the extent of mixing of PCBM is higher in polymers that contain the BT unit than polymers that contain the BO unit. To verify the importance of the benzothiadiazole and benzooxadiazole functionalities in defining the extent of PCBM mixing in these polymers, the solubility limits of PCBM in 2,1,3-benzothiadiazole (BT_m) and 2,1,3-benzooxadiazole (BO_m), which are the monomers of BT and BO unit, was determined using UV–vis spectroscopy. These experiments are carried out at 60 °C, as the melting temperatures of BT_m and BO_m are 42 °C and 52 °C, respectively. From these experiments, the solubility limit of PCBM is found to be 68.0 mg/mL in BT_m and 12.6 mg/mL in BO_m at 60 °C, in agreement with the neutron reflectivity determined solubility limits of PCBM in the low bandgap polymers.

The solubility of carbon nanoparticles in polymers or solvents is often dominated by specific interactions between the nanoparticle and surrounding matrix. For instance, in single walled carbon nanotubes, polymers and solvents capable of π–π interactions and electron donor-acceptor interactions with SWNT walls have been shown to form stable dispersions.[23–25] Other specific interactions that occur between the solvent molecules and nanotube surface may also be important, since the most successful solvents tested have amide structural units, pointing to a specific interaction.[23,24,26] Work by Maeda, et al, studied a series of amines and found that dispersibility decreases in the order of primary, secondary, and tertiary amines.[26] Similarly, work in our group has shown that the presence of a minority of interacting functional groups within a polymer chain leads to an optimum interaction between the polymer and fullerene. Density functional theory calculations that identify the binding energy and geometry of the interaction between the functional monomers and fullerenes correspond very well with the experimental results.[27]

Therefore, one explanation for the different solubility of PCBM in these two similar components is that the BT functional group forms a stronger non-covalent interaction with

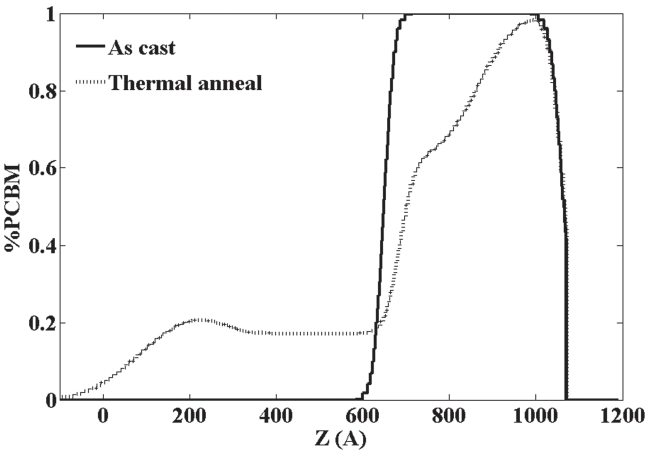

Figure 10. PCBM depth profile of the PCDTBT:PCBM bilayer as cast and thermally annealed as determined from the reflectivity curves shown in 9.

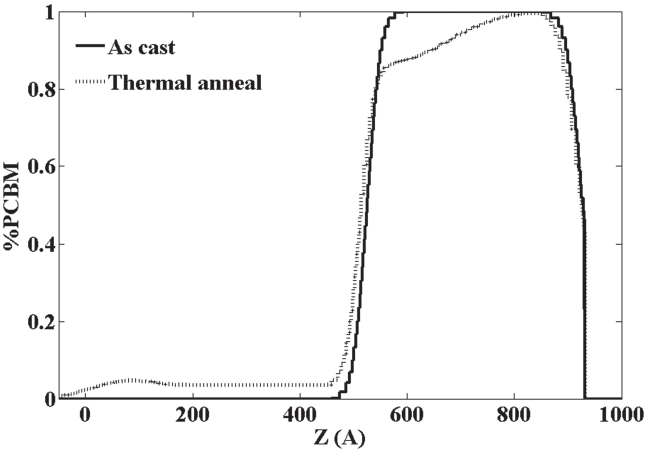

Figure 12. PCBM volume fraction profile of the PCDTBX:PCBM bilayer as cast and thermally annealed as determined from the reflectivity curves shown in Figure 11.

Table 3. Extent of PCBM mixing in the LBG polymers at 140 °C as determined from neutron reflectivity listed with the hole mobility of the LBG polymers as determined with bottom contact TFT measurements.

	PSBTBT (BT)	SOEH (BO)	PCPDTBT (BT)	COEH (BO)	PCDTBT (BT)	PCDTBX (BO)
Extent of mixing, Λ_{PCBM}^{NR} [vol%]	23 ± 2	6 ± 0.5	9 ±1	3 ± 0.5	17 ±1.5	4 ± 0.5
Hole mobility [cm^2/Vs]	2×10^{-3}	1×10^{-3}	3.1×10^{-3}	2.7×10^{-3}	4×10^{-4}	2×10^{-3}

PCBM than the BO functional group does. This is reasonable, as like most fullerenes, PCBM is a very good electron acceptor. Moreover, sulfur (in BT) has a larger electron cloud and a smaller ionization energy than oxygen (in BO), which are indicative of a better electron donor. This should result in a stronger non-covalent interaction between the fullerene and the BT functional group than between the fullerene and BO functional group. This is also consistent with the solubility of C_{60} in similar sulfur and oxygen containing solvents: for instance, C_{60} solubility in CS_2 is 7.9 mg/mL[28] and negligible in supercritical CO_2.[29]

2.6. Crystallinity of LBG Polymers Containing BT and BO Unit

The extent of mixing determined by neutron reflectivity is the extent of PCBM mixing in the LBG layer, which may include both crystalline and amorphous polymer. Thus, the extent of the PCBM mixing, Λ_{PCBM}^{NR}, in the LBG reported above is

$$\Lambda_{PCBM}^{NR} = \frac{\phi_{PCBM}}{\phi_{PCBM} + \phi_{LBG}^{a} + \phi_{LBG}^{c}} \quad (1)$$

where ϕ_{PCBM} is the volume fraction of PCBM in the mixed region, ϕ_{LBG}^{a} is the volume fraction of amorphous conjugated polymer in the mixed region, and ϕ_{LBG}^{c} is the volume fraction of crystalline conjugated polymer in the mixed region. If the fullerene does not penetrate the crystalline portion of the polymer, it is constrained to the amorphous phase of the polymer, and the actual concentration (Λ_{PCBM}) of the fullerene in the amorphous phase is

$$\Lambda_{PCBM} = \frac{\phi_{PCBM}}{\phi_{PCBM} + \phi_{LBG}^{a}} \quad (2)$$

Most importantly, the performance of the OPV active layer depends on the extent of the fullerene mixing in the amorphous phase, Λ_{PCBM}, as this determines the amount of donor-acceptor interface that exists and if there is sufficient fullerene loading to allow effective charge transport across the phase. Thus, if the polymer does not exhibit a crystalline phase, Equation (1) becomes Equation (2) and the extent of mixing determined by neutron reflectivity is the extent of the fullerene mixing in the polymer $\Lambda_{PCBM} = \Lambda_{PCBM}^{NR}$ that is of most interest. If the conjugated polymer does exhibit a crystalline phase, then ϕ_{LBG}^{c} is also needed to transform Λ_{PCBM}^{NR} to Λ_{PCBM}.

To provide this information for the materials studied, grazing incident X-ray scattering was completed to examine the crystallinity of these LBG polymers. Figure S1 shows the GIWAXS results of all the bilayers. No polymers except PSBTBT and SOEH show a strong crystalline peak in these scattering curves, indicating limited ordering in these materials. Thus, for these low-band gap polymers, the extent of mixing that is reported above is the extent of the fullerene mixing in the polymer, and these values can be compared directly.

The PSBTBT and SOEH bilayers exhibit peaks at $q \approx 0.36$ Å^{-1}, which is associated with the (100) crystal planes.[13] It is not surprising to see the similar diffraction patterns for PSBTBT and SOEH, as they have similar chemical structures. Moreover, the similar area of (100) peaks of the thermally annealed PSBTBT and SOEH bilayers is interpreted to indicate that the crystallinity of the polymer does not change significantly when replacing the BT unit with the BO unit, based on the similar structure and densities of PSBTBT and SOEH. Unfortunately, the percent crystallinity cannot be determined from these scattering curves, and thus the exact value of Λ_{PCBM} cannot be determined from the experimentally determined Λ_{PCBM}^{NR}. This, however, does not preclude a qualitative discussion. For instance, the values of Λ_{PCBM}^{NR} that are reported in Table 3 are minimum values for Λ_{PCBM}, as the presence of a crystalline phase in the polymer only increases the value of Λ_{PCBM} from Λ_{PCBM}^{NR}.

The crystallinity of the conjugated polymers can also be indirectly probed by examining the hole transport of the materials, as hole transport occurs more readily in crystalline materials than amorphous materials.[30,31] Thus, the hole mobility of the LBG conjugated polymers is measured and listed in Table 3, where the specific experimental and fabrication procedures are provided in the supplemental information. Similar hole mobilities are found for PSBTBT and SOEH, which is consistent with these two polymers attaining similar levels of crystallinity. Therefore, even accounting for the crystallinity of the conjugated polymers studied, in all cases the extent of PCBM mixing in these low band gap polymers is higher in CPs that contain the BT unit than polymers that contain the BO unit.

2.7. The Relationship Between PCBM Mixing Behavior and OPV Active Layer Structure

The reported results document the tendency of the polymer chains to mix with PCBM when annealed at 140 °C. They do not, however, define the thermodynamic miscibility of PCBM in the low-bandgap polymers, as we were unable to identify a suitable annealing temperature that limits the crystallization of PCBM (<≈150 °C)[32] and is above the glass transition temperature (Tg) of all the polymers. As shown in the Supporting Information, differential scanning calorimetry indicates that only one of the polymers (PCDTBT, Tg = 117 °C) exhibit a Tg between 0 and 250 °C. Despite this limitation, the reported mixing behavior of PCBM and the low-bandgap polymers does provide insight into the structure of OPV active layers as they are

formed by casting from solution. It is important to remember that PCBM is a small molecule relative to the polymer that mixes with a glassy polymer, much like a solvent or plasticizer molecule will. This is verified by the fact that PCBM does mix into all examined polymers at 140 °C, even up to 23% into glassy PSBTBT. To appreciate the relevance of these results to the morphology of a spin-cast active layer, it must be emphasized that the morphology of polymer–fullerene mixture that is spin cast from solution is guided by the mixing behavior of the polymer and fullerene. During spin coating, the morphology of the polymer–fullerene mixture evolves towards its equilibrium structure while there exists sufficient solvent to allow molecular mobility of the polymer and/or fullerene. The timescale of solvent evaporation is usually sufficiently fast that the final structure is far from equilibrium, but the driving force that guides this structural evolution is the mixing behavior of the polymer and fullerene. For instance, a polymer that does not mix with PCBM will form a purer polymer rich phase during drying than one that readily mixes with PCBM. There is a stronger driving force to phase separate in the former than there is in the latter. It is also important to note that results in our lab[33] and reported in the literature[34] clearly indicate that the structure and morphology of P3HT:PCBM active layers continue to evolve long after the solvent has appeared to evaporate, presumably due to trace solvent. This exemplifies the importance of the mixing behavior of the polymer and fullerene in determining the resultant structure and morphology of polymer:fullerene mixtures formed by spin coating. Similarly, the timescale of the thermal annealing process reported above may not produce a final structure that is at equilibrium, but the driving force that guides this structural evolution is also the mixing behavior of the polymer and fullerene. Therefore, the results of the reported neutron reflectivity experiments provide a measure of the tendency of the PCBM to mix with the polymer chain, which is an important indicator of the morphology of the cast BHJ blend, as it guides structural evolution during the casting process. Thus, while the reported results do not provide sufficient detail to predict the exact morphology and phase compositions of a spin coated BHJ, the reported mixing behavior does guide the formation of the BHJ blend film during casting. As such, the reported results provide important structural information of cast bulk heterojunctions that correlates to their OPV performance.

2.8. Correlation of Structure to OPV Function

The results presented here clearly document the mixing behavior and interdiffusion of PCBM in LBG conjugated polymers. The diffusion of PCBM into the LBG conjugated polymers upon thermal annealing was monitored by neutron reflectometry, where the depth profile after annealing clearly shows a plateau region in the central portion of the thin film. This plateau region is the portion of the film that is not influenced by the air or silicon surface, and therefore tracks the extent of PCBM mixing in LBG conjugated polymer. As listed in Table 3, in all cases the extent of PCBM mixing in the BO materials is always significantly less than in the BT materials, which may provide an explanation for the experimentally observed lower power conversion efficiency of active layers that consist of mixture of PCBM with BO based low bandgap conjugated polymers.

The reported variation in polymer:fullerene mixing behavior may provide insight into the fact that OPV active layers that comprise BO containing conjugated polymers do not exhibit an improvement in power conversion efficiency, as would be expected based solely on the V_{oc} of the polymers. For instance, Leclerc and coauthors compared the device performance of PCDTBT:PCBM and PCDTBX:PCBM BHJs, which show that the PCDTBX:PCBM device (V_{oc} = 0.96 V, FF = 0.60) has higher V_{oc} and FF than PCDTBT:PCBM (V_{oc} = 0.86 V, FF = 0.56).[19] Moreover, they have almost the same onset absorption and PCDTBX absorbs more photons than PCDTBT with the same thickness.[19] Additionally, the hole mobility of PCDTBX is superior to that of PCDTBT, as shown in Table 3. However, the performance of the PCDTBX based device is much worse than that of the PCDTBT based device; the PCE of the PCDTBT device is 50% higher than that of the PCDTBX based device.

This performance enhancement is due to the fact that the PCDTBT active layer has a J_{sc} that is twice that of the PCDTBX active layer.[19] Similar results are found when comparing the performance of PCPDTBT vs. COEH or PSBTBT vs. SOEH. For example, a device based on the BO material COEH:PCBM mixture (V_{oc} = 0.78 V)[35] has higher V_{oc} and FF than a device based on the similar BT material, a PCPDTB:PCBM mixture (V_{oc} = 0.62 – 0.66 V),[19,36] where similar hole mobility and absorption exist for this pair.[35] However, the J_{sc} of the COEH based device (J_{sc} = 5.2 mA/cm^2)[35] is much lower than the J_{sc} of the PCPDTBT based device (J_{sc} = 7.0 – 16.2 mA/cm^2).[36] This lower J_{sc} results in a lower PCE of the COEH based device than that of the PCPDTBT based device. Therefore, the poor performance for devices that are based on polymers that contain the BO unit appears to be primarily due to a lower J_{sc}, which is strongly dependent on the morphology of the active layer, as it affects the charge generation, transport and recombination.

To understand the relationship between J_{sc} and charge generation, transport and recombination, the generalized Shockley equation shows the relationship between the current density (J) and voltage (V) in an OPV cell[37]

$$J = \frac{R_p}{R_s + R_p}\left\{J_s\left[exp\left(\frac{q(V - JR_s)}{nk_BT}\right) - 1\right] + \frac{V}{R_p}\right\} - J_{ph}(V) \quad (3)$$

where R_p and R_s are the series and parallel resistances, respectively, J_s is the reverse saturation current density, q is the fundamental charge, n is the diode ideality factor, and $J_{ph}(V)$ is the voltage-dependent photocurrent density. For the short circuit condition (V = 0), as J_s is much less than $J_{ph}(0)$, then $J_{sc} = J_{ph}(0)$.[38] The photocurrent of a space charge that is formed near the anode without considering the recombination of electrons and holes can be expressed as[39–41]

$$J_{ph} = q\left(\frac{9\varepsilon_0\varepsilon_r\mu_h}{8q}\right)^{1/4} G^{3/4}V_1^{1/2} \quad (4)$$

where ε_o and ε_r are the dielectric permittivity of the materials. The dielectric constant ε_r of conjugated polymers is usually 2–4 (i.e. *ca.* 3 for P3HT) and ε_r of PCBM is ca. 3.6.[42,43] Thus,

exchanging the BO unit with a BT unit does not significantly alter ε_r. μ_h is the hole mobility, and G is the generation rate of excitons. This equation does not consider recombination, so all excitons dissociate to free electrons and holes and transport to the electrodes in this model. V_1 is the effective voltage across the device, which = $V_0 - V$, where V_0 is the compensation voltage, which is determined at $J_{ph} = 0$.[38,40–45] V_0 is slightly higher than V_{oc} and increases as V_{oc} increases.[44–46] Hence for the short circuit condition (V = 0),

$$J_{sc} = J_{ph}(0) = q\left(\frac{9\varepsilon_0\varepsilon_r\mu_h}{8q}\right)^{1/4} G^{3/4}V_0^{1/2} \quad (5)$$

Equation 5 predicts that the BO materials e.g. PCDTBX, should have larger J_{sc} based on a higher V_{oc}, better absorption, and higher hole mobility than a BT material, e.g. PCDTBT, assuming no recombination. However, the PCPTBX:PCBM BHJ shows a much lower J_{sc} than the PCPTBT:PCBM BHJ, which can be attributed to more exciton recombination.

The increased recombination of the PCPTBX:PCBM BHJ, and other BO containing materials, is also consistent with the measured amount of fullerene in the mixed phase. The polymer/fullerene mixture phase clearly plays an important role in the exciton dissociation and charge transport, where the dispersed fullerenes create an abundance of donor/acceptor interface, allowing effective exciton dissociation. However, if these acceptors are isolated, as would occur in a system with low loadings of PCBM, the transport of these charges between acceptors becomes limited, creating traps. Also, a low PCBM loading as observed in BO materials, provides inadequate donor/acceptor interface, decreases the probability of the exciton dissociation increasing recombination and resulting in a decrease of internal quantum efficiency and J_{sc}. An increase of PCBM loading increases the amount of donor/acceptor interfaces, resulting in more efficient dissociation of excitons into electrons and holes and provides better transport channels for the separated charges.

Consequently, a conjugated polymer:fullerene BHJ that exhibits low PCBM content in the miscible phase provides a limited amount of "streams" for electron transport, resulting in an increase in the recombination of free charge carriers. Furthermore, in samples with low fullerene loadings, there is a long distance between two adjacent PCBM in the mixed phase, which inhibits electron transport, resulting in an increase of free charge carrier recombination and a decrease of PCE. This is supported by a recent report that monitors the miscibility and morphology of PCBTTPD:PCBM mixtures.[47] The authors claim that the decrease of the PCE in a PCBTTPD:PCBM device with thermal annealing is due to a decrease in the PCBM loading in the mixed region. This deceased loading inhibits electron transport in the mixed region and increases charge-carrier recombination, resulting in a low PCE.

Therefore, the mixing behavior of a fullerene in a conjugated polymer plays an important role in the charge generation and recombination of an OPV BHJ active layer. More importantly, the reported extent of mixing results provide crucial fundamental information that correlates the low extent of PCBM mixing with low band gap polymers that contain the BO unit, explaining their unexpectantly low power conversion efficiencies. More importantly, these results emphasize the fact that the design of low band gap conjugated polymers for optimal OPV performance must target polymers with both desired photo-physical properties and necessary thermodynamic mixing behavior with donors.

3. Conclusion

The depth profile of PCBM in an LBG polymer:PCBM thin film that is formed by thermal annealing an initial well-separated bilayer is determined by neutron reflectometry, where the extent of PCBM mixing in donor–acceptor LBG polymers is obtained. In all cases, the PCBM loading is higher in polymers containing the BT unit than polymers containing the BO unit. Grazing incidence X-ray results show that the crystallinity of LBG polymer is minimal in many of the polymers studied, and does not change much with replacement of the BO and BT units for the PSBTBT/SOEH pair. This allows the direct comparison of the PCBM mixing behavior in the three conjugated polymer pairs that are examined in this study.

These results provide an explanation for the inferior performance of OPV devices that utilized conjugated polymers based on the BO unit. The presence of the BO unit should improve the device efficiency, as its presence increases V_{oc} without significantly altering the absorption onset, hole mobility, and fill factor. This performance is explained as due to the low PCBM loading in the mixed phase, offering limited amount of donor/acceptor interfaces, which decreases the probability of exciton dissociation into free charge carrier. This, in turn, increases exciton recombination, and decreases internal quantum efficiency, which results in a low J_{sc} and PCE. Furthermore, low PCBM loadings provides limited pathways for electron transport in the mixed region, as the increased distance between adjacent PCBM in the miscible phase creates charge traps. The results exemplify the importance of understanding the thermodynamic miscibility of the fullerene and conjugated polymer in designing new conjugated polymers for organic solar cells, as this thermodynamic parameter controls the morphology of the resultant bulk heterojunction.

4. Experimental Section

Materials: PCBM was purchased from Nano-C, and all the low band gap (LBG) conjugated polymers were received from Konarka. 2,1,3-benzothiadiazole (BT_m) and 2,1,3-benzooxadiazole (BO_m), which are the monomers of the BT and BO units, were purchased from Alfa Aesar. The chemical structures, names, abbreviations, molecular weight (M_n), and polydispersity of all the conjugated polymers, 2,1,3-benzothiadiazole and 2,1,3-benzooxadiazole are shown in Table 2. To fabricate the initial bilayers, PCBM (29 mg/mL in *o*-dichlorobenzene) was first spin-coated onto clean silicon wafers at 1000 rpm for 60 seconds. Prior to spin-coating, the silicon wafers are cleaned by immersing in hot piranha (a 3:1 (v/v) mixture of concentrated sulfuric acid and hydrogen peroxide) at ≈70 °C for 15 min, followed by rinsing with copious amounts of high purity water and drying under a stream of nitrogen. The LBG polymers were received from Konarka blade-coated onto a salt plate. The bilayer was obtained by capturing the LBG polymer that was floated onto the surface of high purity water with a PCBM coated silicon wafer. The sample was then dried in air at an angle and then in an unheated vacuum oven for 24 h to removed residual water.

Thermal annealing was performed at 140 °C for 30 min. Previous work has clearly shown that this is adequate time to readily diffuse PCBM into conjugated polymers. For instance, Watts and coworkers report that the diffusion coefficient of PCBM in P3HT is 2.5×10^{-14} m^2/s at 140 °C,[9] which means the PCBM molecule will traverse a 1700 Å film (the thickest film studied) in less than a second. Moreover, Russell and coauthors monitored the diffusion of PCBM into PSBTBT by thermal and found that the interdiffusion was complete in 1 min at 150 °C.[13]

GIWAXS: X-ray diffraction from the thin films is completed with a high resolution one-dimensional Phillips X'pert-Pro diffractometer in grazing-incidence geometry with a wavelength of 0.154 nm. The detector is a point-by-point krypton filled proportional counter. Samples were scanned in z direction and the results are reported as a function of q_z. The angle of incidence between the X-ray and the thin film surface is 0.3° for all samples.

Neutron Reflectometry: All reflectivity measurements were completed on the Liquids Reflectometer at the Spallation Neutron Source at Oak Ridge National Laboratory with a neutron wavelength varying from 2.75–5.75 Å and an effective q-range of 0.006–0.145 $Å^{-1}$($q = 4\pi/\lambda \sin\theta$, where λ is the neutron wavelength and θ is the scattering angle). Layers and Motofit Software were used to fit the measured reflectivity curves,[48,49] providing the reflectivity of a model scattering length density profile, which can be analyzed to determine the structure of the thin films. 2–5 layers were used to model the depth profiles of the as-cast and annealed bilayers. The scattering length density, thickness, and roughness of each layer is freely varied in the fitting procedure. The quality of fit is gauged using mean squared error statistics, combined with a mass balance of the model system to within 5% of the mass balance of the initial bilayer.

The experimentally determined SLD profile is then analyzed to determine the concentration depth profile of each component in the system. For instance, the PCBM concentration depth profile is determined using,

$$\phi(z)_{PCBM} = \frac{\rho(z) - \rho_{Polymer}}{\rho_{PCBM} - \rho_{Polymer}} \quad (6)$$

where $\varphi(z)_{PCBM}$ is the volume fraction of PCBM at depth z, $\rho(z)$ is the experimentally determined scattering length density at depth z, and $\rho_{Polymer}$ and ρ_{PCBM} are the SLD of the LBG polymer and PCBM, respectively. In order to quantitatively analyze the reflectivity curves, the accurate scattering length density of each component is needed. The SLD of amorphous PCBM is determined to be 4.4×10^{-6} $Å^{-2}$ based on its density and composition, and measurements of the reflectivity of spin-cast PCBM monolayers.[5,50,51] The SLD of the LBG polymers are determined by the measurement of the neutron reflectivity of LBG polymer monolayers and verified by calculating the SLDs using the atomic composition of the polymers and their density, which is determined experimentally with pycnometry.

Measurement of Solubility Using UV–Vis Spectroscopy: UV–vis spectra were recorded with a Thermo Scientific Evolution 600 UV–vis spectrophotometer at 60 °C and used to determine the solubility of PCBM in the BT and BO monomers. The Beer–Lambert law describes the linear relationship between the optical density and solution concentration: $D = c \cdot \varepsilon \cdot L$, where D is the measured optical density, c is the concentration of solution, ε is the extinction coefficient, and L is the path-length, which is 1mm in this work. The optical densities at 600 nm of PCBM solutions in BT_m and BO_m of known concentration are measured and plotted as a function of PCBM concentration, and fit to a linear function. To obtain the PCBM solubility limit, an over-saturated solution was first prepared at 60 °C and then quickly filtered through a 200 nm PTFE membrane (preheated to 60 °C) to obtained a saturated solution. The saturated solution is then serially diluted (28×) with BT_m or BO_m respectively. The dilution is necessary because the saturated solution is too dark for transmission of the UV. The optical density of this diluted solution is then recorded, from which the PCBM concentration is determined based on the previously determined extinction coefficient and Beers law. Finally, the PCBM solubility limit is obtained by multiplying this concentration by 28.

Supporting Information

Supporting Information is available from the Wiley Online Library or from the author.

Acknowledgements

The authors wish to acknowledge the Sustainable Energy Education Research Center and the Joint Institute for Neutron Sciences at the University of Tennessee, as well as the National Science Foundation (DMR-1005987) for support of this project. M.D.D. also acknowledges the support of the Department of Energy, Office of Basic Energy Sciences, Division of Materials Sciences and Engineering. The support of the Scientific User Facilities Division, Office of Basic Energy Sciences, U.S. Department of Energy, who sponsors the Oak Ridge National Laboratory Spallation Neutron Source is gratefully acknowledged. Figures 3 and 4 were corrected on September 13, 2013.

Received: March 9, 2013
Revised: May 24, 2013
Published online: September 11, 2013

[1] R. F. Service, *Science* **2011**, *332*, 293.
[2] M. C. Scharber, D. Muhlbacher, M. Koppe, P. Denk, C. Waldauf, A. J. Heeger, C. J. Brabec, *Adv. Mater.* **2006**, *18*, 789–794.
[3] R. Kroon, M. Lenes, J. C. Hummelen, P. W. M. Blom, B. de Boer, *Poly. Rev.* **2008**, *48*, 531–582.
[4] W. Yin, M. D. Dadmun, *ACS Nano* **2011**, *5*, 4756–4768.
[5] H. P. Chen, R. Hegde, J. Browning, M. D. Dadmun, *Phys. Chem. Chem. Phys.* **2012**, *14*, 5635–5641.
[6] N. D. Treat, M. A. Brady, G. Smith, M. F. Toney, E. J. Kramer, C. J. Hawker, M. L. Chabinyc, *Adv. Energy Mater.* **2011**, *1*, 82–89.
[7] D. Chen, A. Nakahara, D. Wei, D. Nordlund, T. P. Russell, *Nano Lett.* **2011**, *11*, 561–567.
[8] B. A. Collins, E. Gann, L. Guignard, X. He, C. R. McNeill, H. Ade, *J. Phys. Chem. Lett.* **2010**, *1*, 3160–3166.
[9] B. Watts, W. J. Belcher, L. Thomsen, H. Ade, P. C. Dastoor, *Macromolecules* **2009**, *42*, 8392–8397.
[10] G. Dennler, M. C. ScharBer, C. J. Brabec, *Adv. Mater.* **2009**, *21*, 1323–1338.
[11] J. H. Hou, H. Y. Chen, S. Zhang, G. Li, Y. Yang, *J. Am. Chem. Soc.* **2008**, *130*, 16144–16145.
[12] S. H. Park, A. Roy, S. Beaupré, S. Cho, N. Coates, J. S. Moon, D. Moses, M. Leclerc, K. Lee, A. J. Heeger, *Nat. Photonics* **2009**, *3*, 297–302.
[13] H. Y. Lu, B. Akgun, T. P. Russell, *Adv. Energy Mater.* **2011**, *1*, 870–878.
[14] T. Wang, A. J. Pearson, A. D. F. Dunbar, P. A. Staniec, D. C. Watters, H. N. Yi, A. J. Ryan, R. A. L. Jones, A. Iragi, D. G. Lidzey, *Adv. Funct. Mater.* **2012**, *22*, 1399–1408.
[15] S. R. Cowan, N. Banerji, W. L. Leong, A. J. Heeger, *Adv. Funct. Mater.* **2012**, *22*, 1116–1128.
[16] B. A. Collins, Z. Li, C. R. McNeill, H. Ade, *Macromolecules* **2011**, *44*, 9747–9751.
[17] R. C. Coffin, J. Peet, J. Rogers, G. C. Bazan, *Nat. Chem.* **2009**, *1*, 657–661.
[18] C. V. Hoven, X. D. Dang, R. C. Coffin, J. Peet, T. C. Nguyen, G. C. Bazan, *Adv. Energy Mater.* **2010**, *122*, E63–E66.
[19] N. Blouin, A. Michaud D.Gendron, S. Wakim, E. Blair, R. Neagu-Plesu, M. Belletete, G. Durocher, Y. Tao, M. Leclerc, *J. Am. Chem. Soc.* **2008**, *130*, 732–742.
[20] A. J. Parnell, A. D. F. Dunbar, A. J. Pearson, P. A. Staniec, A. J. C. Dennison, H. Hamamatsu, M. W. A. Skoda, D. G. Lidzey, R. A. L. Jones, *Adv. Mater.* **2010**, *22*, 2444–2447.

[21] J. W. Kiel, B. J. Kirby, C. F. Majkrzak, B. B. Maranville, M. E. Mackay, *Soft Matter* **2010**, *6*, 641–646.
[22] J. W. Kiel, A. P. R. Eberle, M. E. Mackay, *Phys. Rev. Lett.* **2010**, *105*, 168701.
[23] S. D. Bergin, Z. Sun, D. Rickard, P. V. Streicj, J. P. Hamilton, J. N. Coleman, *ACS Nano* **2009**, *3*, 2340–2350.
[24] Q. Cheng, S. Debnath, E. Gregan, H. J. Byrne, *J. Phys. Chem. C.* **2010**, *114*, 8821–8827.
[25] D. Linton, P. Driva, B. Sumpter, I. Ivanov, D. Geohegan, C. F. Feigerle, M. D. Dadmun, *Soft Matter* **2010**, *6*, 2801–2814.
[26] Y. Maeda, S. Kimura, Y. Hirashima, M. Kanda, Y. Lian, T. Wakahara, *J. Phys. Chem. B.* **2004**, *108*, 18395–18397.
[27] S. L. Teh, D. Linton, B. Sumpter, M. D. Dadmun, *Macromolecules* **2011**, *44*, 7737–7745.
[28] R. S. Ruoff, D. S. Tse, R. Malhotra, D. C. Lorents, *J. Chem. Phys.* **1993**, *97*, 3379–3383.
[29] A. N. Khlobystov, D. A. Britz, J. W. Wang, S. A. O'Neil, M. Poliakoff, G. A. D. Briggs, *J. Mater. Chem.* **2004**, *14*, 2852–2857.
[30] H. Sirringhaus, P. J. Brown, R. H. Friend, M. M. Nielsen, K. Bechgaard, B. M. W. Langeveld-Voss, A. J. H. Spiering, R. A. J. Janssen, E. W. Meijer, P. Herwig, D. M. de Leeuw, *Nature* **1999**, *401*, 685–688.
[31] V. D. Mihailetchi, H. X. Xie, B. de Boer, L. J. A. Koster, P. W. M. Blom, *Adv. Funct. Mater.* **2006**, *16*, 699–708.
[32] E. Verploegen, R. Mondal, C. J. Bettinger, S. Sok, M. F. Toney, Z. Bao, *Adv. Funct. Mater.* **2010**, *20*, 3519–3529.
[33] R. Hegde, N. Henry, B. Whittle, H. Zang, B. Hu, J. Chen, K. Xiao, M. Dadmun, *Solar Energy Materials and Solar Cells* **2012**, *107*, 112–124.
[34] L. Chang, H. W. A. Lademann, J.-B. Bonekamp K. Meerholz A.J. Moule *Adv. Funct. Mat.* **2011**, *21*, 1779–1787.
[35] J. C. Bijleveld, M. Shahid, J. Gilot, M. M. Wienk, R. A. J. Janssen, *Adv. Funct. Mater.* **2009**, *19*, 3262–3270.
[36] J. Peet, J. Y. Kim, N. E. Coates, W. L. Ma, D. Moses, A. J. Heeger, G. C. Bazan, *Nat. Mater.* **2007**, *6*, 497–509.
[37] H. R. Bube, A. L. Fahrenbruch, Advances in Electronics and Electron Physics, Academic, New York **1981**, p. 163.
[38] M. D. Perez, C. Boren, S. R. Forrest, M. E. Thompson, *J. Am. Chem. Soc.* **2009**, *131*, 9281–9286.
[39] A. M. Goodman, A. Rose, *J. Appl. Phys.* **1971**, *42*, 2823–2930.
[40] M. S. Roy, P. Balraju, U. S. Deol, S. K. Sharma, G. D. Sharma, *J. Mater. Sci.* **2008**, *43*, 5551–5563.
[41] V. D. Mihailetchi, J. Wildeman, P. W. M. Blom, *Phys. Rev. Lett.* **2005**, *94*, 126602.
[42] G. Li, R. Zhu, Y. Yang, *Nat. Photonics* **2012**, *5*, 153–161.
[43] J. W. Jung, W. H. Jo, *Adv. Funct. Mater.* **2010**, *20*, 2355–2363.
[44] V. D. Mihailetchi, L. J. A. Koster, J. C. Hummelen, P. W. M. Blom, *Phys. Rev. Lett.* **2004**, *93*, 216601.
[45] J. S. Yu, J. Huang, L. Zhang, Y. D. Jiang, *J. Appl. Phys.* **2009**, *106*, 063103.
[46] J. K. J. van Duren, X. N. Yang, J. Loos, W. T. Bulle-Lieuwma, A. B. Sieval, J. C. Hummelen, R. A. J. Janssen, *Adv. Funct. Mater.* **2004**, *14*, 425–434.
[47] J. A. Bartelt, Z. M. Beiley, E. T. Hoke, W. R. Mateker, J. D. Douglas, B. A. Collins, J. R. Tumbleston, K. R. Graham, A. Amassian, H. Ade, J. M. J. Frechet, M. T. Toney, M. D. McGehee, *Adv. Energy. Mater.* **2012**, 10.1002/aenm.201200637.
[48] Layers is an Excel spreadsheet for modeling NR data developed by John Ankner at Oak Ridge National Laboratory.
[49] A. Nelson, *J. Appl. Cryst.* **2006**, *39*, 273–276.
[50] H. P. Chen, S. Hu, H. D. Zang, B. Hu, M. Dadmun, *Adv. Funct. Mater.* **2013**, *13*, 1701–1710.
[51] H. P. Chen, J. H. Chen, W. Yin, X. Yu, M. Shao, K. Xiao, K. L. Hong, D. L. Pickel, W. M. Kochemba, S. M. Kilbey II, M. Dadmun, *J. Mater. Chem. A* **2013**, *1*, 5309–5319.